
Article:
Stone, E.J.W., Panagiotou, P.A., Mühlthaler, J. et al. (2025) Degradation-informed coil insulation modelling by impedance frequency response analysis. IEEE Transactions on Industry Applications (99). pp. 1-12. ISSN: 0093-9994

https://doi.org/10.1109/tia.2025.3645167

Degradation-Informed Coil Insulation Modelling by Impedance Frequency Response Analysis

Edward J.W. Stone, Panagiotis A. Panagiotou, *Member, IEEE*, Johannes Mühlthaler, *Member, IEEE*, Andrew R. Mills, Alexis Lambourne, Geraint W. Jewell

***Abstract*—The highly demanding operation of electrical machines in aerospace ultimately leads to the degradation of the electrical insulation system within the machine stator windings over time. This paper presents a novel hybrid methodology for high-frequency modelling of the insulation system in the concentrated stator winding of a 2 MW aerospace generator. A degradation-informed coil model is presented for purposes of characterisation and monitoring of the coil insulation system by the impedance responses using Bode plots in frequency response analysis (FRA), notably electrical impedance spectroscopy. The proposed approach utilises a finite element model which is informed by measurements of dielectric properties on unaged and thermally aged insulation material specimen and deployed in tandem with an electrical equivalent circuit representation. An analytical tool built in Matlab is used to quantify the results taken from finite element modelling and implemented into LTSpice for circuit considerations, so that the model considers mutual coupling effects of inductances and high-frequency effects such as proximity and skin effect. Dielectric properties measurements allow to inform this model to account for degradation effects and how these reflect in the impedance frequency spectrum. This novel methodology allows extraction of the impedance profile with respect to the material changes within the simulated and experimentally measured unaged and degraded insulation system. The theoretical results acquired by the hybrid co-simulations are validated experimentally using thermally aged coil samples.**

***Index Terms*— stator winding insulation, dielectrics, electrical impedance spectroscopy, finite element analysis, permittivity.**

I. Introduction

To meet global CO2 emissions targets, the transportation sector, such as electric vehicles, railway, the more-electric aircraft, and various aerospace applications, is becoming more and more electric. Electrical machines are critical for the successful advancement of these technologies. Insulating systems for electrical machines are key elements in electrified propulsion in terms of safety, reliability, and efficiency [1]. The physical size of electrical machines is reducing to meet the higher power density requirements by reducing weight. The need for reliable and robust insulation systems is paramount for such safety-critical applications to prevent catastrophic failures like short-circuits [1]-[2]. As such, insulating components for electrical machines are being studied with continuously increasing research interest. This research field spans many aspects including design and material selection, inspection and testing, health monitoring, degradation, and estimation of remaining useful life [3]-[4].

The key factors that have a direct impact on the insulation life are stresses due to thermal, electrical, ambient and mechanical stresses, often encountered in literature as T.E.A.M. stresses [1], [5]-[6]. Within aerospace applications this means that there is always a tangible effect from all these stresses in tandem. The demand for higher torque, results in greater currents through the machine stator winding, while the high frequency switching from inverters initiates *dv/dt* shocks that lead to PD inception. The latter effect is intensified as the ambient condition of low atmospheric pressure at high altitudes reduces the threshold of the PD inception voltage due to Paschen's Law [7]. These electrical ageing factors increase the winding temperature, resulting in gradual or accelerated thermal degradation. At the same time, changing altitudes and environmental temperatures may alter the profile of the insulation in terms of material properties and degradation rate. Along with mechanical stresses from loading conditions and vibrations, insulating components such as the turn insulation are susceptible to treeing and cracking, whereas hotspots can result in failure of the groundwall insulation. Ultimately, any of these faults at incipient level will evolve to a high-severity fault, risking the electrical machine reliability and the end-user safety.

Several studies have been published on the testing and inspection of insulation systems in electrical machines, as well as on the health monitoring and the estimation of degradation. Visual inspection, initial characterisation, and pass/fail testing by IEEE/IEC standards are in place during manufacture and factory acceptance testing [8]-[9]. Beyond these, continuous condition monitoring may be deployed during in-service operation, often combined with either on-wing or off-wing

This work was supported by the Aerospace Technology Institute (ATI UK) and Innovate UK/UKRI under the project REPLENISH (Grant 10112182).

Corresponding author: Panagiotis A. Panagiotou

E. J. W. Stone is with the School of Electrical and Electronic Engineering, University of Sheffield, S1 3JD, Sheffield, U.K., (e-mail: e.j.stone@sheffield.ac.uk).

P. A. Panagiotou is with the School of Electrical and Electronic Engineering, University of Sheffield, S1 3JD, Sheffield, U.K. (e-mail: p.panagiotou@sheffield.ac.uk).

J. Mühlthaler is with the School of Engineering and Design, Technical University of Munich (TUM), 85748, Garching, Germany (e-mail: johannes.muehlthaler@tum.de).

A. R. Mills is with the School of Electrical and Electronic Engineering, University of Sheffield, S1 3JD, Sheffield, U.K. (e-mail: a.r.mills@sheffield.ac.uk).

A. Lambourne is with Rolls-Royce Central Services, Rolls-Royce Plc UK, DE24 9HY, Derby, U.K. (e-mail: Al.Lambourne@rolls-royce.com)

G. W. Jewell is the School of Electrical and Electronic Engineering, University of Sheffield, S1 3JD, Sheffield, U.K. (e-mail: g.jewell@sheffield.ac.uk).

inspections. Representative studies for PD detection have been published in works such as [10] and [11] for inverter-fed operation and aerospace components at low pressure, representing high altitude insulation degradation mechanisms. Other studies have presented monitoring of insulation health condition and degradation, by the extraction of common mode characteristics under normal and inverter-fed operation in [12]-[14].

Amongst the current technologies developed for the inspection of insulation systems and components, electrical impedance spectroscopy (EIS) is a broadly deployed method that is based on the acquisition of the impedance frequency response by a broad-spectrum frequency sweep under fixed-amplitude or variable excitation. By doing so, the impedance of the component under test is acquired and handled as a transfer function allowing its characterisation by means of the amplitude and phase responses. These can then be visualised via the well-known Bode plots [15]. In the last decade, EIS has been continuously deployed as an inspection technique, mainly on ex-situ applications due to its non-destructive nature, simplicity in terms of instrumentation, and low-cost implementation [16]-[17]. Novel research in the field is continuously improving the technique in terms of accuracy, instrumentation, and more in-situ application [18]-[19].

EIS is widely deployed for extraction of key parameters to reliably model elements of electrical machine windings and coil assemblies. Thus far, stator coil insulation systems are modelled by deploying either finite element modelling (FEM) for physics-based analysis, or electrical equivalent circuit-based representations for data-based analysis. The combinations thereof in a co-simulation setting are known as hybrid modelling [18]. Additionally, Ruiz-Sarrio et al present in [20] a comparison of different modelling types, showing the benefits of different simulation frameworks. The novelty of this hybrid co-simulation framework addresses a gap in the current state of the art that is based upon the combination of three systems; with real-world degraded material properties fed into the model by dielectric measurements, in tandem with the utilisation of the FEM analysis and the equivalent circuit, allow the prediction of thermal degradation on coils insulation systems. Representative studies using the discussed methods of insulation modelling are published in [20]-[24] for concentrated winding insulation, in [25]-[27] for distributed winding insulation, and in [28]-[30] for hairpin and diamond shaped coils. There are different Although the discussed studies encompass reliable modelling approaches by different tools, there is still a significant research gap regarding the combined modelling of degradation effects and the mapping of changes in the material properties with respect to the impedance frequency responses during the degradation. To achieve reliable representation and mapping of the behaviour and profiling of insulation systems with respect to changes in the material properties, it is critical to deploy models that encompass FEM modelling and a detailed electrical equivalent representation in a co-simulation fashion, so that different types of information can be exchanged for each modelling component during the insulation degradation.

This paper presents a novel modelling methodology via a hybrid co-simulation framework for stator coil insulation in electrical machines. The co-simulation framework incorporates FEM coupled with a detailed electrical equivalent circuit representation. Whereas the hybrid approach entails informing the model with measurements of dielectric permittivity of thermally aged insulation material samples that correspond to the insulation system of the coil. This modelling framework creates an active feedback loop that feeds the thermal degradation mechanism and its characteristics back into the co-simulation via the dielectric measurements. The proposed methodology is demonstrated on the insulation system of a stand-alone coil. The coil is from the stator winding of the 2MW permanent magnet generator in a hybrid aircraft demonstrator [15], [31]-[32].

The work within this paper examines the modelling of the dynamic changes to the insulation system using impedance frequency response analysis (FRA). This will characterise the changes in the material properties within the different insulation layers for the beneficial profiling of the thermal degradation mechanism. Through this paper the term FRA is used instead of EIS as a naming convention, as the paper's aim is to evaluate the dynamic changes to the resonant frequencies due to the material properties changing, rather than just characterisation of a coil. This paper builds upon the co-simulated framework originally presented in [18], however, now the co-simulation framework is adapted into a hybrid co-simulated framework that incorporates real-world measured material properties to aid in the modelling of degradation effects. The results acquired from the proposed hybrid co-simulation methodology are validated with experimental measurements acquired on healthy as-manufactured coils and thermally aged coil assemblies that were initially presented in [19] and [31]. The proposed measurement-informed hybrid approach enables reliable and accurate modelling for insulation monitoring and degradation assessment purposes in electrical machine windings. The remainder of this paper is organised as follows. Section II presents the characterisation and modelling of electrical insulation systems, with information on the insulation material and FRA. Section III describes the modelling procedure and experimental methodology, discussing the modelling approach used to represent material changes over time. Section IV introduces the results of the impedance frequency response analysis (FRA) method and its application for evaluating insulation condition. Finally, Section V summarizes the main findings and provides conclusions drawn from this study.

II. Characterisation and Modelling of Electrical Insulation Systems

A. Electrical Insulation Materials and Properties

Electrical insulation within an electrical machine is made up of several different components. A combination of these components makes up an insulation system that is required to give high quality electrical protection in terms of, endurance, dielectric strength, and the absorption of mechanical and thermal stress. The typical materials for insulation systems within electrical machines are shown in Table I [1], [2], [4].

TABLE I
TYPICAL INSULATION MATERIALS [1], [2], [4]

Components	*Materials*
Strand Insulation	Polyamide-imide/polyimide/polyester or glass fabric tape
Turn Insulation	Kapton/polyimide/mica/epoxies
Groundwall Insulation	Mica/ PET/epoxy resins
Slot Insulation	Impregnated PET/Nomex/mica
Slot Wedge	Silicone/glass filled epoxies
Semiconductive Coating & PD protection	Single array containing the frequencies for modelling.
VPI varnish and resin-rich material combinations	Varnishes/alkyd resins/silicone resins/polyester/polyester-imide/polyurethane

The combination of materials within the insulation system of a coil are broadly made from components in the strand insulation, turn insulation, ground wall insulation and the semiconductive coating sections. The slot insulation and slot wedges are primarily insulation material that forms part of the stator slots and is integrated into the insulation system of the coils when the coils are placed into the stator, in the case of concentrated windings. When these windings are integrated into the stator slots and the different slot insulations are in place, it is common practice for a form of vacuum pressure infiltration (VPI) resin to be applied to the winding and slot insulation system, which is a universal procedure for high performance machines. The primary function of this process is to eliminate air voids, which will ensure an enhanced dielectric and mechanical strength, as well as improved resilience to moisture and environmental factors in aerospace applications.

In electrical machines, there is a large volume of research dedicated to thermal modelling and thermal management. By [33], thermal sources within the machine consist of iron loss, copper loss and high-frequency loss. High-frequency losses can come in the form of copper losses and iron losses. For high-frequency copper losses, the issue arises from increased skin and proximity effects with increasing operating frequency. Meanwhile, high-frequency losses can manifest as high-frequency eddy currents within the laminations of the rotor/stator cores, causing iron losses due to high frequency currents [34], [35]. These cause a rise in the overall temperature of the machine, leading to faster insulation degradation and winding failure. To counteract this, different thermal management and cooling methods are deployed to remove heat and excess thermal fluctuations [36].

B. Winding Insulation and Modelling of Material Changes

Thus far, it has been seen by the literature that the key stress aspect for electrical machine windings is thermal degradation due to increased temperature in tandem with electrical and mechanical stresses. With the exposure to temperature, the electrical insulation material properties diminish, and hence the insulating system degrades. While the reduction of heat and the subsequent thermal effects are well-known and ongoing challenges within insulation systems and high-voltage machine design, the overall effect of higher temperature on the material properties within the insulation system is less known and understood in integrated coil assemblies. In [37], a comprehensive study is provided on the effects of the relative permittivity (RP) of epoxy mica insulation tape when exposed to thermal aging. This exposure resulted in a gradual reduction of the relative permittivity with respect to aging. The reduction was in part attributed to the post-curing effect and formation of voids within the insulation epoxy. The incomplete curing of epoxy resins during manufacturing stage causes the discussed post-curing effect, which restarts the curing process when insulation is subjected to the thermal levels witnessed within the machine [38]. Such imperfections and the associated phenomena contribute to the reduction of relative permittivity in the insulation system layers. A compelling analysis is presented in [39] explaining the effect of reducing relative permittivity in the insulation material on the electric field strength around the conductors and the insulation system of a cable assembly. The latter study determined that as the relative permittivity is reduced, the electric field strength is varied.
With reference to electrical machines, the first and last turn of a coil will see a variation of capacitance due to the geometrical changes and permittivity reduction caused by thermal aging. This phenomenon can be observed between the coil and the stator core, or between the turns of the coil (turn-to-turn). This variation in the distribution and magnitude of the electric field can alter and decrease the capacitive effects between the winding and the core or between the adjacent turns due to the relationship between capacitance C and the electric field strength E. This is shown by:

$$C = Q/(E \cdot d) \,, \tag{1}$$

where Q is the electric charge, E the electric field strength and d the distance between conductors. Here, d can also represent the thickness of insulating elements or the thickness of the different layers in the insulation system depending how the distance of the conductors is defined. In terms of an electrical equivalent circuit for a tested insulation system or coil assembly, the impedance of a coil can be expressed in terms of the coil inductance L, resistance R, and the capacitance C of (1). A key challenge in the modelling of stator winding coils and their insulation is the consideration of both the electromagnetic (FEM) model in combination with a reliable electrical equivalent to acquire critical values of the coil circuit. Although the direct modelling of phenomena such as ageing and stresses is not possible, a significant contribution can be found in reliable models for emulation of similar effects that reflect the influence of changes in the material characteristics. The aim of frequency response-based characterisation like EIS is to identify characteristics and map the behaviour of changing material properties in the physical representation, i.e., FEM model, and the electrical equivalent circuit.

C. Impedance Frequency Response Analysis (FRA)

The examination of the impedance response over frequency has provided valuable results for the characterisation of insulation systems and materials. By utilising Bode plots, this type of analysis allows a visualisation of the impedance

amplitude and phase angle over the frequency spectrum. This allows identification of the resonance characteristics as well as any elements of change within the electrical equivalent circuit for the component or system under test. The impedance Z is acquired under a low voltage excitation as a function of the voltage over current flowing through the component. This is represented by:

$$Z(\omega) = |Z| \angle\varphi = Re\{Z\} + j \cdot Im\{Z\} , \quad (2)$$

where $|Z|$ is the impedance magnitude, and φ the phase. The amplitude and phase parts of (2) are evaluated individually by separate Bode plots. As shown in several published works, changing the properties of the dielectrics within insulation systems results in a change of the resistive, capacitive, and inductive elements encapsulated in the real and imaginary parts of the complex impedance expressed by (2). These changes are reflected in the Bode plots through an increase in the peak impedance and shifts of the resonant frequency at that maximum peak. This paper presents a novel method for modelling this complex behaviour within the material properties.

III. Modelling Procedure and Experimental Methodology

A. High-Frequency Modelling and FEM setting

The FEM discussed in this paper needs to consider all the proximity and skin effects of the Litz wire strands within the turns over the full frequency sweep range. High-frequency modelling of windings presented in [23], [40]-[41] refer to the skin effect within single conductors as a significant issue regarding the high-frequency behaviour within motor windings. The model uses a frequency domain FEA and as the resonant frequency locations for these coils are roughly known due to the experimental results, hence the frequency sweep is set about the resonant frequency. For example, if the resonant frequency is at 2MHz, the frequency sweep is set between 1MHz and 3MHz. The more frequency points taken between these values the more accurate the depiction of the resonant frequency will be; however, the longer the simulation will take to complete. The results in this paper were achieved using 33 simulation frequency points, one at each end frequency, one at the centre point where the location of the desired frequency is expected to be, and then 15 for either side of the centre frequency. As a practice, this method serves well in plotting resonant frequencies. More frequency points over this short frequency range offered no greater accuracy. Fig. 1 illustrates a 2D cross-section of the coil examined in this paper (Fig. 1a) and the insulation system components (class H insulation) with different colour annotations as described through Fig. 1b. The copper bundles (orange in Fig. 1a) are separated by the turn insulation (black in Fig. 1a) which is a polyimide film (class H Kapton tape). The groundwall insulation consists of two layers (purple & green areas in Fig. 1b) which are of the same material as each other, notably multilayer glass cloth mica paper, impregnated with thermosetting epoxy resin and enhanced by a layer of polyethylene terephthalate film as the thermoplastic polymer. The turn-to-turn and groundwall insulation material properties are utilised for simulation within this paper, being the materials that are thermally aged and measured to inform this hybrid model. Due to the negligible length of the end-winding vs the active length for these coils, the active length was instead taken as the length as though the coils would have been cut down the centre of the end windings. The addition of a very small length to the 2D model length was therefore added.

The coil's turn bundles, depicted in the orange areas of Fig. 1b, are made from 350 enamel wire Litz strands per turn. It was necessary to model the overall turns material properties changes, due to the skin effects from the Litz wire bundles and the effect they would have on each turn. Initially, these effects were calculated at each discrete frequency point using another FEM model that outputs the relative permeability of the bundled copper wire conductors at each desired frequency. As this process involves the skin and proximity effects between each turn, the mesh in this simulation was redefined at each frequency point, for finer meshing at each step. The skin depth was first calculated and then the mesh was set to 8 times the skin depth (i.e., 8 mesh elements across the skin depth) to adequately capture phenomena of interest. This can cause problems within the model itself, since as the frequency increases and the skin depth decreases the mesh will refine more and more, leading to increased solving times. A mesh refinement multiplier of 8 times the skin depth provided the best trade-off between accuracy and solver time for this model geometry.

The discussed FEM component provides the material properties information for lumped modelling of Litz wire turns and was derived from the initial analysis presented in [42]. This frequency-dependent output array is inserted into the material properties for the turns in the two main FEM coil models. The insulation material is also analysed with a mesh that is 8 times the skin depth of a conductor. This approach renders a reliable representation of the high-frequency behaviour of the coil with regards to the copper conductors and insulation. After this initialisation, a validation takes place by the dielectric measurements described later in Section III-C. Then, the model is further informed by these measurements to input in the model the values of permittivity acquired from the thermally aged insulating layer material specimen. As a last step after all data have been collated, the coil global impedance is extracted to visualize via the frequency response. The latter is then compared with measurements of coil assemblies as will be described in Section III-C.

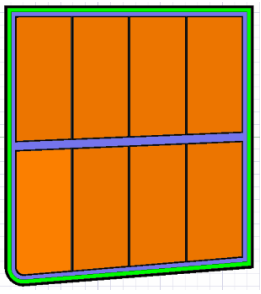

Colour	Object
Orange	Turn (copper Litz bundle)
Internal Black	Turn-turn insulation
Purple	Ground wall insulation layer 1
Green	Ground wall insulation layer 2
External Black	PD shielding

a) b)

Fig. 1. Coil model: a) 2D FEM structure, and b) description of insulation system components.

B. Co-Simulations of FEM with Electrical Equivalent Circuit

As mentioned in the previous subsection, the initial FEM analysis evaluates relationships between conductors and insulation layers within the geometric confines of the coil structure. As a second stage, an equivalent circuit is used to collate all the different relationships derived by the Ansys software package and build the final high-frequency parameter setting. The code developed for the latter calculation of electrical parameters also generates the spectroscopic response over the required frequency range. The FEM model is split into two different simulations within Ansys Maxwell 2D. The first model is based on the eddy-current solver of Ansys Maxwell, and focuses on deriving the resistances, inductances and mutual coupling information for the 2D coil geometry shown in Fig. 1.

The second FEM simulation is based upon the AC conduction solution in the same software package and is focused on solving the electrostatic variations for the conductance's and capacitive effects through the individual insulation layers between turns. The solver outputs the resistive part of this solution as a conductance (*1/R*) as it is working in electrostatics mode and that facilitates more efficient differentiation. This part is acknowledged in the LTSpice model as a resistance (*1/G*). The output results from these FEM simulations are in the form of *nxn* reduced matrices, *n* being the number of turns in a coil. There is one for each of the resistive, inductive, mutual coupling, conductive and capacitive effects within the coil geometry and between the subsequent insulation layers. The end effects are not considered as the model deploys geometry in 2D representation. This approach imposes a trade-off in terms of end-winding considerations to reduce design and computational complexity as well as to reduce simulation times. However, as will be shown in Section IV via the co-simulation results and the experimental measurements, this approach renders accurate and representative results as the size of active length vs the end-windings deem these effects near negligible.

Both FEM components in this model deal with two parts of the same problem at set frequency points. To evaluate the spectroscopy waveforms an electrical equivalent circuit model was designed to correlate both FEM components' values at each measured frequency point. Fig. 2 depicts the LTSpice model equivalent circuit that has been developed to represent the geometric structure, as well as the capacitive and inductive interactions within the designated coil. In [40], a concept was formed for a structural design of an equivalent circuit representing a coil assembly with similar structure. In [41]-[44], the authors present similar equivalent circuitry models to approach impedance sweep responses for the modelling of stator poles and winding insulation. The design in Fig. 2 builds on these works to allow for the incorporation of greater detail within the impedance spectroscopy results. It draws on the mutual inductances and capacitive coupling due to geometric placement of turns within the coil, and these are further informed by the co-simulation model and reinforced by the dielectric measurements. In the first degradation modelling iteration the FEM was modified by a scaling-up factor of 0.15 to account for volume changes in the geometries of the insulating layers due to thermal expansion.

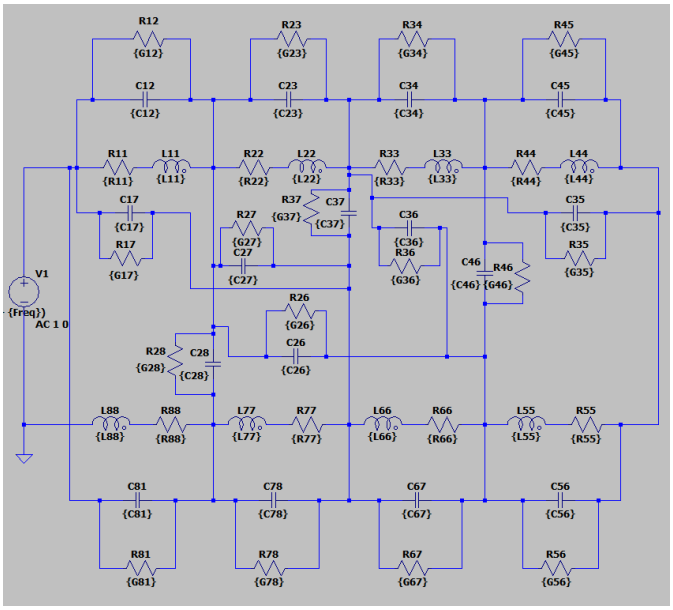

Fig. 2. Equivalent circuit model for the representation of the examined 8-turn coil utilised in the co-simulation model.

The equivalent circuit shown in Fig 2 shows a number of named components. These represent the different measured FEM results per frequency point. For example, R11 and L11 are the self-resistance and inductance of turn 1 respectively. C12 is representing the capacitive effects between turns 1 and 2, whereas R12 is representing one over the conductance between turns 1 and 2. To this end, all the number labels for the components follow the same naming convention. The matrices calculated by the two FEM simulations are initially processed in Matlab. This ensures that each matrix representing a different component is separated into a frequency-dependent array of a single column. In Table II, the different types of arrays extracted with this process are presented. In this table, under "description", the bracketed value is in reference to the component name and is shown in the electrical equivalent circuit representation of Fig. 2. There is one frequency-dependent array for each component. Hence, (*Rxx*) by way of example, could be in reference to *R11,* or *R22*, etc., shown in the equivalent circuit. The final step in this part of the methodology sees the final analysis of these arrays using the equivalent circuit. Matlab utilises the Netlist functionality in LTSpice to use batch files and build a new circuit. This new Netlist has all the component values for a desired frequency point. LTSpice then builds the equivalent circuit to use these component values in simulation. The result at this frequency point is then fed back into Matlab and stored in a results array. The process repeats using the next frequency point, forming a changeable resolution by varying the number of frequency points required in Ansys. The results array can then plot the Bode plot using the impedance magnitude and phase to show the characterisation spectrum of the examined coil.

TABLE II
TYPES OF ARRAYS USED IN THE CALCULATIONS PROCESS OF THE EQUIVALENT CIRCUIT MODEL

Modelling Arrays		
Name of Array	***Frequency Dependent***	***Description***
Resistance	Yes	Arrays containing Resistance values (*Rxx*)
Inductance	Yes	Arrays containing Inductance values (*Lxx*)
Inductive Mutual Coupling	Yes	Arrays containing Inductive coupling values (*Kxx*)
Conductance	Yes	Arrays containing Conductance values (*Gxx*)
Capacitance	Yes	Arrays containing Capacitance values (*Cxx*)
Frequency	–	Single array containing the frequencies for modelling

C. Test Hardware and Experimental Measurements

Two different sets of test hardware and instrumentation were utilised for experimental measurements. These hardware set-ups are shown in Fig. 3. The dielectric fixture WK–1020 shown in Fig. 3a was used to measure the relative permittivity of the material samples shown in Fig. 3b. The samples are of a known thickness and placed between the brass plates shown in the test fixture in Fig. 3a. Initially, these measurements were performed at healthy (unaged, at time zero) stage. The samples were then thermally aged using the ovens of Fig. 3c, for 100-hour intervals at 200°C which is slightly above the rated 180°C temperature for class H insulation. The choice of temperature was made to accommodate for thermal stresses slightly above the rated temperature, whilst allowing gradual degradation effects rather than accelerated thermal ageing, which can alter and compromise the insulation degradation profile [19], [44]. The test procedure in this experiment is the same as the one described by [19] and [45], to ensure the material properties degradation was the same as the one described in the coils insulation system presented in the latter references. Every 100 hours of thermal degradation, the dielectric properties of each specimen were measured and recorded, to inform the FEM model described through Section III-A and account for degradation effects within the co-simulation setting. From the materials shown in Fig. 3b, the specimens labelled with numbers 1 and 4 (pointed at with arrows) are part of the examined coil insulation system, being the turn-to-turn insulation (Kapton tape) and the groundwall insulation (Mica film layers).

The impedance analyser WK6500B shown in Fig. 3d was used to acquire the impedance responses by impedance spectroscopy for the coil assemblies of Fig. 3e by the same process as described in [19], [31], [45]. Table III indicatively presents values for every 500 hours of thermal ageing for the dielectric property of interest to inform the co-simulation model's material library while accounting for the thermal degradation effects. These are the relative permittivity values measured with the dielectric fixture at different frequencies. In Table III, when comparing values across a row, there is minimal change in the permittivity values with respect to frequency. There is a small frequency dependent change when moving from lower frequency to high frequency that is to be expected. At higher frequency, the unimportant second decimal point change that occurs between 1MHz and 5MHz is likely due to the sensitivity of the equipment and is insignificant when compared to the thermal degradation change over time. However, this is not the case for the hours of ageing. Comparing across columns for the same materials, significant changes are observed in the permittivity values compared over the duration of the ageing process. This demonstrates the tangible impact of thermal stresses over the frequency effects in terms of dielectric properties changes.

Fig. 3. Test hardware and instrumentation used for experimental measurements on coils and insulation materials: a) WK–1020 dielectric fixture unit for relative permittivity measurements, b) specimens of insulation materials measured with the dielectric fixture at 100-hour intervals of thermal degradation, c) ovens used for thermal degradation [19], [45], d) impedance analyser WK–1J6500B for impedance spectroscopy measurements [19], [45], e) thermally aged coil assemblies under test, inside the thermal degradation oven [19], [45].

TABLE III
MEASURED VALUES OF RELATIVE PERMITTIVITY IN THE TURN AND GROUNDWALL INSULATION LAYERS

Ageing Hours	Insul. Layer	1 kHz	100 kHz	1 MHz	2 MHz	3 MHz	4 MHz
0	Kapton	3.31	3.31	3.30	3.31	3.31	3.32
0	Mica	3.80	3.69	3.68	3.68	3.69	3.70
100	Kapton	3.23	3.22	3.21	3.22	3.23	3.23
100	Mica	3.70	3.66	3.65	3.66	3.66	3.66
500	Kapton	2.65	2.58	2.58	2.57	2.59	2.59
500	Mica	3.68	3.63	3.62	3.63	3.63	3.63

Ageing Hours	Insul. Layer	1 kHz	100 kHz	1 MHz	2 MHz	3 MHz	4 MHz
1000	Kapton	2.20	2.19	2.19	2.20	2.20	2.21
1000	Mica	3.65	3.62	3.62	3.61	3.62	3.62

IV. Results and Discussion

A. Diminishing Properties in the Turn-to-Turn Coil Insulation

This first study examines the reduction of relative permittivity in the turn-turn insulation tape through the co-simulation model only. This is the black tape shown between the turns in Fig. 1. The ground wall tape, shown as the green and purple tape, layers 1 and 2 in Fig. 1, are kept at a fixed value of R_p=*6.5*. The relative permittivity value is reduced over a set range, simulating changes in the Mica impregnated epoxy resin tape, for values of relative permittivity ranging from *9* to *4*. This is derived on the information studied on similar aspects of property changes presented in [23], [43], [46]. This provides an evidence-informed selection from the overview of different types of insulating tapes in terms of dielectric property values and frequency response, due to the relative permittivity value as it is thermally aged or undergoes changes in its structural properties that will affect its material response [41], [47].

Fig. 4 and Fig. 5 show the results of this study, notably the impedance magnitude of the first resonant peak and the corresponding impedance phase angle across the resonant peak, respectively. Through Fig. 4, as the relative permittivity of the turn-to-turn insulation drops the first resonant peak increases in frequency from 1.3MHz to 1.6MHz. The phase responses, shown in Fig. 5, show that as the resonant point is reached the system translates from inductive to capacitive which is indicative of the first resonance. It is known that decreasing capacitance between turns causes the resonant peak to increase and shift in frequency [19], [38], [43]-[47]. Hence, from the previous discussion on material properties, as the relative permittivity increases the turn-to-turn capacitance decreases, resulting in the responses shown in Fig. 4 and Fig. 5.

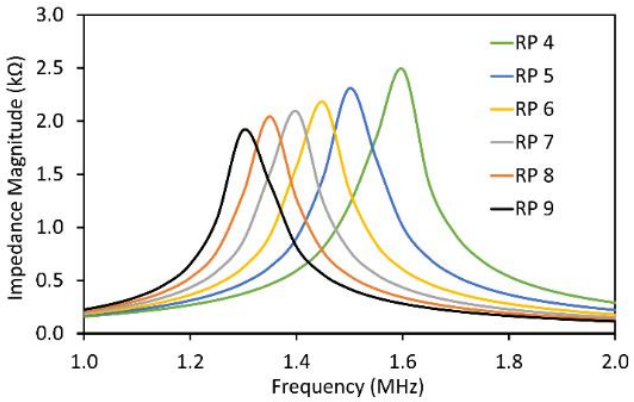

Fig. 4. Coil model impedance amplitude responses with gradual changes in the relative permittivity of the turn-to-turn insulation.

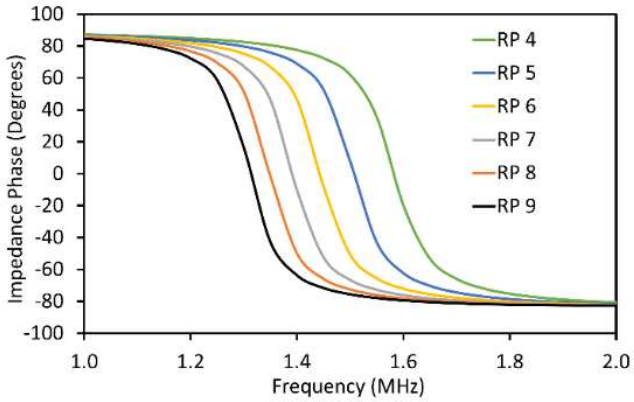

Fig. 5. Coil model impedance phase responses with gradual changes in the relative permittivity of the turn-to-turn insulation.

B. Diminishing Properties in the Groundwall Insulation

This section examines the effect of the same relative permittivity changes, this time in the groundwall insulation layer, in relation to the fixed value of turn-to-turn insulation tape layer. Here the turn-to-turn insulation is kept fixed to a relative permittivity value of *6.5* and the relative permittivity of the groundwall insulation is gradually reduced from a value of *9* to *4*, which is the reverse process from the previous section. The magnitude of the first resonance peak is shown in Fig. 6, whereas Fig. 7 illustrates the corresponding phase response. The reduction in relative permittivity shows a similar increase in the impedance spectra by the first resonant peak as to that captured in the previous subsection. The difference with the previous case study is that the magnitude of the impedance at the peak is initially greater for the higher values of relative permittivity. The incline made by the increasing impedance as the relative permittivity drops is also less when the turn-to-turn insulation permittivity is of fixed value compared to the case where the groundwall is of fixed value. This shows that the turn-to-turn insulation has a higher effect on impedance than the groundwall. This observation is self-consistent, as the turn-to-turn insulation is in close proximity to the turns and will affect the mutual capacitive coupling between the turns with a more tangible impact in the impedance spectrum. This is also due to the geometric design of the examined coil, in the sense that the insulation between turns 1–4 and 5–8 is a lot thinner and stretched over a greater distance than the groundwall that is a lot thicker and covers less distance across each of these turns.

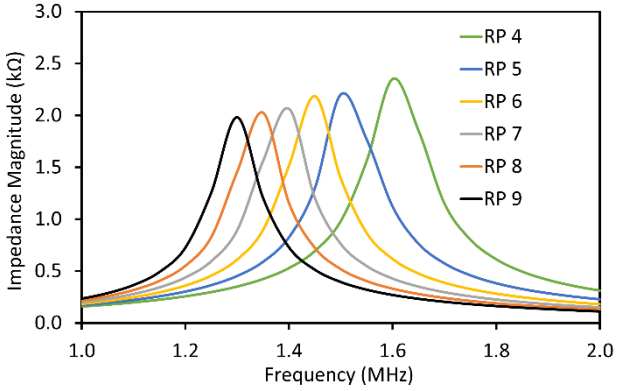

Fig. 6. Coil model impedance amplitude responses with gradual changes in the relative permittivity of the groundwall insulation.

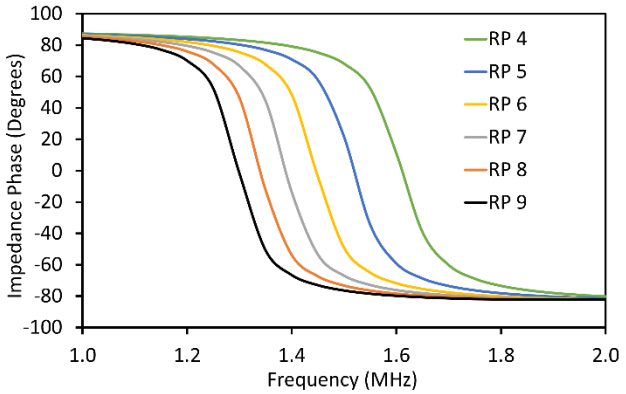

Fig. 7. Coil model impedance phase responses with gradual changes in the relative permittivity of the groundwall insulation.

C. Diminishing Properties of the Overall Coil Insulation System

This section examines results which incorporate the two previous studies. Whereas previously the model had one fixed insulation parameter and the other parameter changing, this case simulates both parameters changing at a fixed rate. The rationale is to examine the frequency responses of the insulation system within the coil during material properties changes, similar as during ageing by thermal exposure, structural changes such as expansion, etc. As mentioned in Section II-B, the geometry of the coil's FEM component in the co-simulation is adapted by scaling to account for changes in volume due to thermal expansion in tandem with the dielectric changes. The permittivity of both the groundwall insulation layers and the turn-to-turn insulation are reduced by 10% of the original value per simulation. By [48]-[49], an average value of different epoxy mica insulation tapes is attributed a value between *5* and *3* for relative permittivity. Therefore, the initial value for the turn insulation was set to *4.5* and the groundwall to *3.4*.

Fig. 8 shows the effect that the gradual 10% reductions have on the magnitude of the first resonant peak. Fig. 9 shows the corresponding impedance phase. These results are taken at a lower permittivity value to the previous case studies, hence the increase in resonant frequency as the permittivity drops is greater than what was seen in the previous two cases. These results show an increase by the same frequency shift as the previous ones where the permittivity values were reduced separately. This is an expected effect of changing all values at the same time, as both material properties will be in effect simultaneously. Another observation compared to the previous cases is that the peak impedance is higher, however the trend is in line with the prior monotonically increasing impedance.

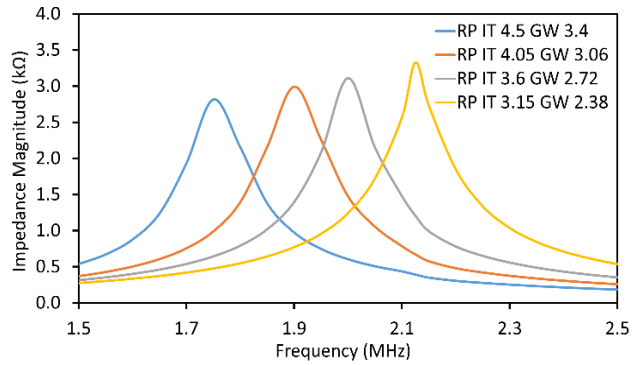

Fig. 8. Coil model impedance amplitude responses with simultaneously applied gradual changes in the permittivity of the turn and the groundwall insulation.

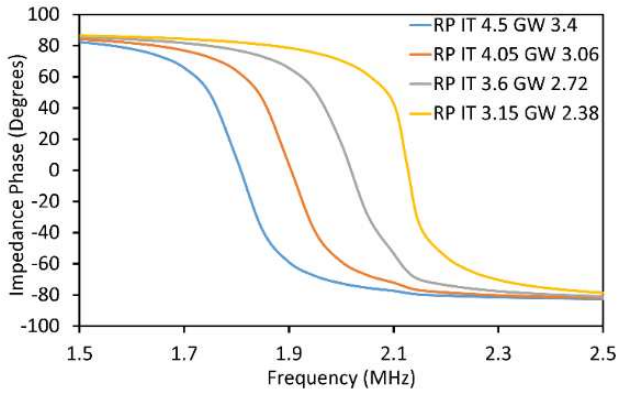

Fig. 9. Coil model impedance phase responses with simultaneously applied gradual changes in the permittivity of the turn and the groundwall insulation.

D. Degradation-informed Model Output and Comparison of Results with measurements of thermally aged coils

This section presents the output of the degradation-informed co-simulation and compares the results against measurements of impedance spectroscopy from thermally aged coils. Fig. 10 shows the frequency response of the impedance amplitude of the coil using the presented co-simulation approach. In Fig. 10, the responses correspond to the impedance amplitude of the coil after informing the materials library of the co-simulation framework with dielectric measurements of the degraded samples at 0 hours (black, T0), 100 hours (blue, T100), 500 hours (red, T500), and 1000 hours (orange, T1000). The acquired responses yield representative results as they encapsulate the changes of the individual material layers simultaneously into one co-simulation that is enhanced by the material properties changes via the measured dielectrics.

Impedance spectroscopy measurements were performed on physical coil assemblies from the 2MW permanent magnet generator of hybrid aircraft demonstrator machine [15], [19] [31], [32]. The batch of coils subjected to thermal degradation was also used and extensively described in [19], [31] and then used for further investigations in this paper. Fig. 11 presents the results for one of the samples from the batch described in [19], [31]. Since all coils are identical and have similar responses as detailed in these references, impedance spectroscopy can be used as an inspection tool in the assessment of health and useful life. The impedance amplitude responses measured on the representative coil from the batch are shown in Fig. 11. The colour-coded curves correspond to the responses measured at the same ageing intervals as accounted for in the model described previously in the co-simulation results of Fig.10 by degrading the insulating material samples.

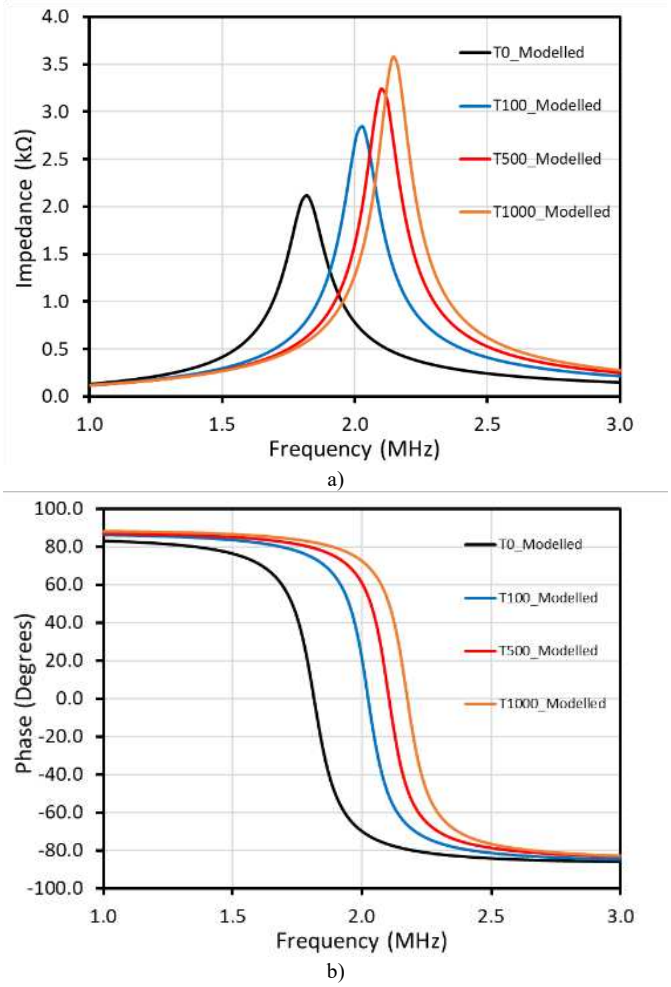

Fig. 10. Co-simulation output: impedance amplitude response after informing the model at 0 hours (unaged, black), 100 hours (blue), 500 hours (red) and 1000 hours (orange) of thermal ageing in the insulation material specimen.

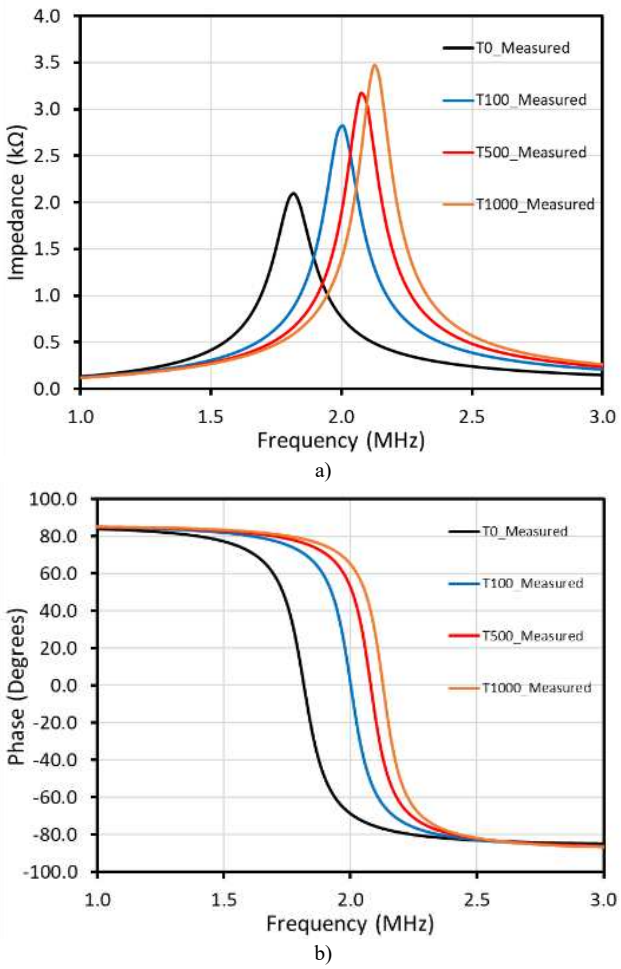

Fig. 11. Impedance amplitude response measured on the healthy (unaged) and thermally aged coil as per the developed co-simulation model: 0 hours (unaged, black), 100 hours (blue), 500 hours (red) and 1000 hours (orange) of thermal ageing in the insulation material specimen.

As can be seen through Fig. 10 and Fig. 11, the proposed degradation-informed co-simulation model predicts the responses measured on the physical coils accurately. All the measured responses on the physical coil during degradation match with consistency the co-simulation outputs both in values of amplitude as well as in terms of the frequency shifts imposed by the degradation mechanisms. It is also seen from Fig. 10 that the impedance trendline retains its monotonically increasing characteristics with respect to the material changes accounted for during degradation, while the modelled and measured results agree with similar recent findings in the literature. These findings are rather compelling and demonstrate the accuracy and versatility of the proposed modelling approach for this type of windings and stator coils. They also form the basis for the potential future development of a line-side modelling tool for health assessment and degradation evaluation during routine inspection of stator winding coils in-shop or in-service.

V. Conclusions

This paper presented a novel hybrid methodology for the degradation-informed modelling of a stator coil insulation system using a co-simulation framework that was exploited with coil impedance frequency response analysis. The characterisation and monitoring of the coil insulation system were facilitated by the impedance responses using Bode plots. In the proposed framework, a finite element model was coupled with an electrical circuit equivalent of the coil accounting for high-frequency phenomena via the coupled models in an iterative simulation process. Additionally, the co-simulation setting was informed by dielectric measurements on material samples to account for changes in the dielectric properties of the insulation layers during thermal degradation. The outputs of the developed co-simulation framework were compared against experimental measurements on the insulation systems of the stator coils coming from the concentrated stator winding of a 2 MW aerospace generator. The theoretical results from the co-simulations were found to predict with a high degree of accuracy the physical coil measurements and consistently match the insulation degradation profile extracted from the amplitude and phase responses experimentally. Through the presented modelling methodology, extraction of the impedance

profiles is enabled in a hybrid manner with respect to the material changes during degradation. This modelling framework renders additional contribution to knowledge in terms of enabling a modelling tool that accounts for degradation effects in tandem with circuit representation and high-frequency phenomena considerations. It also forms the foundation for developing a line-side modelling tool for health assessment and evaluation of insulation degradation during routine in-service inspection of stator winding coils, or during in-shop maintenance.

REFERENCES

[1] G. C. Stone, I. Culbert, E. A. Boulter and H. Dhirani, Electrical insulation for rotating machines: design, evaluation, aging, testing, and repair, Toronto: Wiley-IEEE Press, 2014.

[2] R. Hemmati, F. Wu and A. El-Refaie, "Survey of Insulation Systems in Electrical Machines," in 2019 IEEE International Electric Machines and Drives Conference (IEMDC), San Diego, 2019.

[3] V. Madonna, P. Giangrande and M. Galea, "Electrical Power Generation in Aircraft: Review, Challenges, and Opportunities," IEEE Transactions on Transportation Electrification, vol. 4, no. 3, pp. 646-659, 2018.

[4] M. Borghei and M. Ghassemi, "Insulation materials and systems for more and all-electric aircraft: A review identifying challenges and future research needs," IEEE Transactions on Transportation Electrification, vol. 7, no. 3, pp. 1930-1953, 2021.

[5] P. A. Panagiotou, A. Lambourne and G. W. Jewell, "Survey of Insulation in Electrical Machines for Aerospace: Systems, Materials & Inspection," in 2022 International Conference on Electrical Machines (ICEM).

[6] H. A. Toliyat, S. Nandi and S. Choi, Electric Machines: Modeling, Condition Monitoring, and Fault Diagnosis, CRC Press, 2017.

[7] W. J. Carey, A. J. Wiebe, R. D. Nord and L. L. Altgilbers, "Characterization of Paschen curve anomalies at high PD values," in 2011 IEEE Pulsed Power Conference, Chicago, 2011.

[8] "IEEE Std 1068 -Standard for the Repair and Rewinding of AC Electric Motors in the Petroleum, Chemical, and Process Industries," IEEE.

[9] H. Haghighi, I. Cotton, R. Gardner and B. Sauvage, "Definitions of Test Conditions for High Voltage Aerospace Systems Using the IAGOS Atmospheric Dataset (No. 2018-01-1931).," SAE Technical Paper, 2018.

[10] T. Billard, T. Lebey and F. Fresnet, "Partial discharge in electric motor fed by a PWM inverter: off-line and on-line detection," IEEE Transactions on Dielectrics and Electrical Insulation, vol. 21, no. 3, pp. 1235-1242, 2014.

[11] R. Gardner, I. Cotton and M. Kohler, "Comparison of power frequency and impulse based Partial Discharge measurements on a variety of aerospace components at 1000 and 116 mbar," 2015 IEEE Electrical Insulation Conference (EIC), pp. 430-433, 2015.

[12] I. Tsyokhla, A. Griffo and J. Wang, "Online Condition Monitoring for Diagnosis and Prognosis of Insulation Degradation of Inverter-fed Machines," IEEE Transactions on Industrial Electronics, vol. 66, no. 10, pp. 8126-8135, 2018.

[13] H. Chen, Y. Yan and H. Zhao, "Extraction of Common-Mode Impedance of an Inverter-Fed Induction Motor," IEEE Transactions on Electromagnetic Compatibility, vol. 58, no. 2, pp. 599-606, 2016.

[14] F. Alvarez-Gonzalez, D. Hewitt, A. Griffo and J. Wang, "Challenges of Common Mode Current and Voltage Acquisition for Stator Winding Insulation Health Monitoring," 2020 IEEE Energy Conversion Congress and Exposition (ECCE), pp. 4452-4459, 2020.

[15] P. A. Panagiotou, A. Lambourne and G. W. Jewell, "Ex-situ Inspection of Concentrated Stator Coils by Means of Impedance Spectroscopy," in 2022 International Conference on Electrical Machines (ICEM), Valencia, 2022.

[16] H. Gerengi, "The Use of Dynamic Electrochemical Impedance Spectroscopy in Corrosion Inhibitor Studies," Protection of Metals and Physical Chemistry of Surfaces, vol. 54, no. 3, pp. 536-540, 2018.

[17] F. Ciucci, "Modeling electrochemical impedance spectroscopy," Current Opinion in Electrochemistry, vol. 13, pp. 132-139, 2019.

[18] E. J. Stone, P. A. Panagiotou, J. Mühlthaler, A. R. Mills, A. Lambourne, & G. W. Jewell. "Modelling of Insulation in Concentrated Stator Coils for Characterisation and Material Changes". In 2024 International Conference on Electrical Machines (ICEM) (pp. 01-08). IEEE. (2024, September).

[19] E. J. Stone, P. A. Panagiotou, J. Mühlthaler, A. Reeh, A. Lambourne, & G. W. Jewell. "Thermal degradation profile mapping in stator coil insulation by impedance spectroscopy". IEEE Trans. on Ind. Appl., 2025.

[20] J. E. Ruiz-Sarrio, E. J. Stone, A. R. Mills, J. A. Antonino-Daviu, A. Lambourne, P. A. Panagiotou, "High-Frequency Numerical Modelling for Impedance Frequency Response in Electrical Machine Stator Coils–A Comparative Study". In 2025 IEEE Symposium on Diagnostics for Electric Machines, Power Electronics and Drives (SDEMPED) (pp. 1-7). IEEE. (2025, August).

[21] D. Roger, M. Toudji, S. Duchesne and G. Parent, "Concentrated winding machines fed by PWM inverters: insulation design helped by simulations based on equivalent circuits," in 2017 IEEE Conference on Electrical Insulation and Dielectric Phenomenon (CEIDP), Fort Worth, 2017.

[22] H. Zeng, J. Swanke, T. M. Jahns and B. Sarlioglu, "High-Frequency Modeling and Inter-Turn Voltage Distribution Analysis of a Modular Electric Machine for Electric Aircraft Propulsion," in 2022 IEEE Transportation Electrification Conference & Expo (ITEC), Anaheim, 2022.

[23] J. E. Ruiz-Sarrio, F. Chauvicourt and C. Martis, "Sensitivity Analysis of a Numerical High-Frequency Impedance Model for Rotating Electrical Machines," in 2022 Intern. Conference of Electrical Machines (ICEM).

[24] X. Fan, D. Li, R. Qu and C. Wang, "A Dynamic Multilayer Winding Thermal Model for Electrical Machines with Concentrated Windings," IEEE Trans. on Industrial Electronics, vol. 66, no. 8, pp. 6189-6199, 2019.

[25] Q. Chen, Y. Fan, J. Chen and Y. Lei, "A New Analytical Thermal Model of Distributed Winding Wheel Machine for Electric Vehicles," IEEE Trans. on Vehicular Technology, vol. 71, no. 12, pp. 12691-12700, 2022.

[26] P. Mellor, R. Wrobel and N. Simpson, "AC Losses in High Frequency Electrical Machine Windings formed from Large Section Conductors," in 2014 IEEE Energy Conversion Congress and Expo (ECCE), Pittsburgh.

[27] A. Hoffmann and B. Ponick, "Statistical Deviation of High-Frequency Lumped Model Parameters for Stator Windings in Three-Phase Electrical Machines," in 2020 International Symposium on Power Electronics, Electrical Drives, Automation and Motion (SPEEDAM), Sorrento, 2020.

[28] F. Zhang, D. Gerada, Z. Xu and C. Liu, "A Thermal Modeling Approach and Experimental Validation for an Oil Spray-Cooled Hairpin Winding Machine," IEEE Transactions on Transportation Electrification, vol. 7, no. 4, pp. 2914-2926, 2021.

[29] J. Nonneman, T. Schoonjans, I. T'Jollyn, A. Selema and R. Sprang, "Thermal Property Determination of Different Electric Machine Wire Types by Model Variable Fitting on Measurements," in 2022 International Conference on Electrical Machines (ICEM), Valencia, 2022.

[30] M. Pastura, S. Nuzzo, D. Barater and G. Fanceschini, "Analysis of Voltage Distribution and Connections within a High-Frequency Hairpin Winding Model," in 2022 International Conference on Electrical Machines (ICEM).

[31] P. A. Panagiotou, E. J. Stone, J. Mühlthaler, A. Reeh, A. Lambourne, & G. W. Jewell, (2023, August). Thermal Degradation Profile of Concentrated Stator Winding Insulation by Impedance Spectroscopy. In 2023 IEEE 14th International Symposium on Diagnostics for Electrical Machines, Power Electronics and Drives (SDEMPED) (pp. 554-560).

[32] J. K. Nøland, M. Leandro, J. A. Suul, & M. Molinas, (2020). High-power machines and starter-generator topologies for more electric aircraft: A technology outlook. IEEE access, 8, 130104-130123.

[33] Y. Yang, B. Bilgin, M. Kasprzak, S. Nalakath, H. Sadek, M. Preindl, J. Cotton, N. Schofield and A. Emadi, "Thermal management of electric machines," IET Electrical Systems in Transportation, vol. 7, no. 2, pp. 93-178, 2017.

[34] R.Piotr Wojda, & M. Kazimierz Kazimierczuk, (2012). "Proximity-effect winding loss in different conductors using magnetic field averaging". COMPEL-The international journal for computation and mathematics in electrical and electronic engineering, 31(6), 1793-1814.

[35] S. Jiao, X. Liu, & Z. Zeng, (2017). "Intensive study of skin effect in eddy current testing with pancake coil". IEEE Transactions on Magnetics, 53(7), 1-8.

[36] R. Wrobel, "Thermal management of electrical machines for propulsion – challenges and future trends," Archives of Electrical Engineering, vol. 71, no. 1, pp. 175-187, 2022.

[37] N. Mondal, N. Haque, S. Dalai, S. Chakravorti and B. Chatterjee, "Method for identifying ageing in epoxy-mica composite insulation used in rotational machines through modelling of dielectric relaxation," High Voltage, vol. 5, no. 2, pp. 184-190, 2020.

[38] Y. Jia, Y. Jiang, J. Yang and G. Zhang, "Research on Thermal Aging Properties of Composite Insulating Materials in High Voltage Switchgear," in International Conference on Advances in Energy and Environmental Science (ICAEES), Zhuhai, 2015.

[39] L. Liao, T. Xue, J. Xiong and B. Lu, "Research on the Influence of the Relative Permittivity of the Reinforced Insulation of the Cable Intermediate Joint on the Electric Field Intensity". Journal of Physics: Conference Series, 2021.

[40] Y. Moreno, A. Egea, G. Almandoz, G. Ugalde, A. Urdangarin and R. Moreno, "High-Frequency Modelling of Electrical Machines for EMC Analysis," MDPI Electronics, vol. 787, no. 13, 2024.
[41] K. Vanthuyne, M. Gulec and P. Sergeant, "High-Frequency Motor Modelling: Parameter Variation due to Manufacturing," in International Conference of Electrical Machines (ICEM), Valencia, 2022.
[42] D. A. Hewitt, S. Sundeep, J. Wang and A. Griffo, "High Frequency Modeling of Electric Machines Using Finite Element Analysis Derived Data," IEEE Transactions on Industrial Electronics, vol. 71, no. 2, pp. 1432-1442, 2024.
[43] Y. Kemari, G. Teyssedre, A. Mekhaldi, & M. Teguar, (2020, July). Dielectric properties and β-relaxation in cross-linked polyethylene: Effect of thermal aging. In 2020 IEEE 3rd International Conference on Dielectrics (ICD) (pp. 73-76). IEEE.
[44] N. Ravanis, A. Douvaras, & K. N. Gyftakis, (2025). "New Experimental-Based Modelling of Traction Motor Stator Poles and Windings for Impedance Spectroscopy Analysis". IEEE Trans. on Industry Applications.
[45] E. J. Stone, P. A. Panagiotou, J. Mühlthaler, A. R. Mills, A. Lambourne, G. W. Jewell, (2024, September). Identification of thermal failure profiles in stator winding insulation by impedance spectroscopy. In 2024 International Conference on Electrical Machines (ICEM) (pp. 1-7). IEEE.
[46] J. Pihera, R. Polansky, P. Prosr, & J. Ulrych (2012, October). Dielectric spectroscopy of thermally aged insulation. In 2012 Annual Report Conference on Electrical Insulation and Dielectric Phenomena (pp. 862-865). IEEE.
[47] O. Michal, & V. Mentlík (2018, September). Influence of Thermal Degradation on the Dielectric Properties of Polymer Composites. In 2018 International Conference on Diagnostics in Electrical Engineering (Diagnostika) (pp. 1-5). IEEE.
[48] The Engineering ToolBox. (2010). "Relative permittvity-the dielectric constant". [Online]. Available:
[49] A. V. Hippel, Dielectric materials and applications, The MIT Press, 1952.

Edward J. W. Stone received the B.Eng. degree in electrical engineering from Sheffield Hallam University, Sheffield, U.K., in 2016, and the Ph.D. degree in synchronous reluctance machines from the Department of Electronic and Electrical Engineering of the University of Sheffield, Sheffield, U.K., in 2021.

Since receiving his Ph.D. degree in 2021, he is a Postdoctoral Research Associate with the Electrical Machines and Drives research group of the School of Electrical and Electronic Engineering of the University of Sheffield, Sheffield, U.K., working at the Rolls-Royce University Technology Centre in Advanced Electrical Machines of the University of Sheffield. His research interests include electrical machine design, Class D amplification, insulation monitoring and degradation, as well as inspection and repair technologies for electrical machines.

Dr. Stone is a member of the Institution of Engineering and Technology (IET, U.K.).

Panagiotis A. Panagiotou (M'22) received the 5-year Diploma (B.Eng. & M.Eng.) from the Department of Electrical and Computer Engineering of the University of Patras, Patras, Greece, in 2015, and the M.Sc. degree in Complex Systems and Network Theory from the Department of Mathematics of the Aristotle University of Thessaloniki, Thessaloniki, Greece, in 2017. He received the Ph.D. degree in fault diagnostics of electrical machines from Coventry University, Coventry, U.K., in 2020.

In 2021, he joined the Department of Electronic and Electrical Engineering of the University of Sheffield, Sheffield, U.K., as a postdoctoral research associate at the Rolls-Royce University Technology Centre for Advanced Electrical Machines of the University of Sheffield. Since 2022, he is a Lecturer in electrical machines with the School of Electrical and Electronic Engineering of the University of Sheffield, Sheffield, U.K. His research interests include condition monitoring, fault detection and diagnostics in electrical machines, signal processing for diagnostics, and technologies for the inspection and repair of electrical machines.

Dr. Panagiotou is a member of the IEEE, a member of the Institution of Engineering and Technology (IET, U.K.) and a Fellow of the Higher Education Academy (FHEA), U.K.

Johannes Mühlthaler (Student Member, IEEE, 2024) received the B.Eng. degree in electrical engineering from the University of Applied Sciences, Rosenheim, Germany, in 2017, and the M.Sc. degree in electrical engineering from the Technical University of Munich, Munich, Germany, in 2020.

In 2019, he joined Rolls-Royce Electrical Ltd & Co KG in Munich, Germany where he is currently a doctoral candidate working toward the Ph.D. degree with Technical University of Munich, Munich, Germany, and Rolls-Royce Electrical Ltd. & Co. Deutschland in Munich, Germany. His current research focuses on the modelling and verification of winding fault effects, fault detection and mitigation strategies in multi-lane permanent magnet synchronous machines.

Andrew R. Mills received the MEng degree in control systems and the PhD degree in control and monitoring system engineering from the University of Sheffield, Sheffield, UK, in 2003 and 2013, respectively. After working in the defense industry, he was a Senior Research Fellow at the University of Sheffield with a portfolio of aerospace research in application systems engineering, sensing and data-driven decision making to the application of safety-critical system through-life optimization.

Since 2025 he is a professor of Innovation in Aerospace Systems Monitoring and Control with the School of Electrical and Electronic Engineering of the University of Sheffield. He is the deputy director of the University of Sheffield Rolls-Royce University Technology Centre in Controls and Systems Engineering which seeks to use control systems engineering principles to a broad range of applied control and health management research challenges.

Alexis Lambourne received the B.Eng. degree in materials engineering from Loughborough University, U.K., in 1999 and the Ph.D. degree from Oxford University, Oxford, U.K., in 2003. He joined Rolls-Royce Submarines in 2003, and since 2005 he has been working for Rolls-Royce Plc. Central Technologies as a materials specialist in novel and emerging materials technologies.

From 2014-2017, he held a Royal Society industrial fellowship on the materials challenges for hybrid aerospace. His research focuses on the materials and manufacturing of high-power density electrical systems in aerospace environments, including materials selection, testing, degradation, inspection, and recycling. His research interests include a wide variety of functional, smart, and nano materials as well as their applications in aerospace and electric power systems.

Geraint W. Jewell received the B.Eng. and Ph.D. degrees in electrical engineering from the University of Sheffield, Sheffield, U.K., in 1988 and 1992, respectively. Since 1994, he has been a member of the academic staff with the School of Electrical and Electronic Engineering of the University of Sheffield, where he is a professor of electrical engineering.

He held an Engineering and Physical Sciences Research Council (EPSRC) Advanced Research Fellowship from 2000 to 2005 and a Royal Society Industry Fellowship with Rolls-Royce from 2006 to 2008. He is currently the director at the Rolls-Royce University Centre in Advanced Electrical Machines of the University of Sheffield, and the director at the EPSRC Future Electrical Machines Manufacturing Hub. His research interests include the modelling and design of a wide variety of electromagnetic devices, notably electrical machines for aerospace, electro-mechanical actuators, and high-temperature applications.